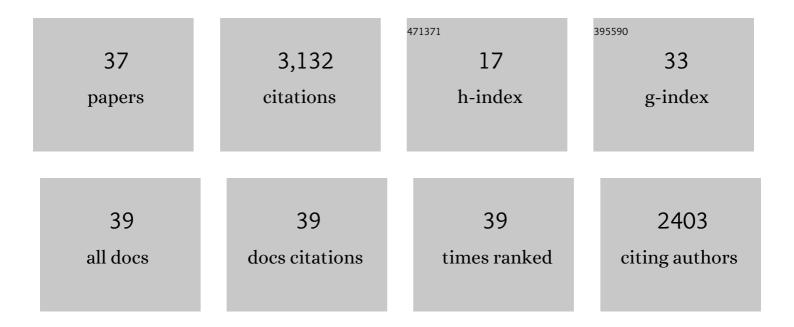
Ludovic de Rochefort

List of Publications by Year in descending order

Source: https://exaly.com/author-pdf/1180850/publications.pdf Version: 2024-02-01



#	Article	IF	CITATIONS
1	Quantitative susceptibility map reconstruction from MR phase data using bayesian regularization: Validation and application to brain imaging. Magnetic Resonance in Medicine, 2010, 63, 194-206.	1.9	567
2	Morphology enabled dipole inversion for quantitative susceptibility mapping using structural consistency between the magnitude image and the susceptibility map. NeuroImage, 2012, 59, 2560-2568.	2.1	397
3	Calculation of susceptibility through multiple orientation sampling (COSMOS): A method for conditioning the inverse problem from measured magnetic field map to susceptibility source image in MRI. Magnetic Resonance in Medicine, 2009, 61, 196-204.	1.9	377
4	A novel background field removal method for MRI using projection onto dipole fields (PDF). NMR in Biomedicine, 2011, 24, 1129-1136.	1.6	352
5	Morphology enabled dipole inversion (MEDI) from a singleâ€angle acquisition: Comparison with COSMOS in human brain imaging. Magnetic Resonance in Medicine, 2011, 66, 777-783.	1.9	290
6	Quantitative MR susceptibility mapping using pieceâ€wise constant regularized inversion of the magnetic field. Magnetic Resonance in Medicine, 2008, 60, 1003-1009.	1.9	247
7	Nonlinear Regularization for Per Voxel Estimation of Magnetic Susceptibility Distributions From MRI Field Maps. IEEE Transactions on Medical Imaging, 2010, 29, 273-281.	5.4	192
8	An illustrated comparison of processing methods for phase MRI and QSM: removal of background field contributions from sources outside the region of interest. NMR in Biomedicine, 2017, 30, e3604.	1.6	124
9	In vitro validation of computational fluid dynamic simulation in human proximal airways with hyperpolarized 3He magnetic resonance phase-contrast velocimetry. Journal of Applied Physiology, 2007, 102, 2012-2023.	1.2	85
10	<i>In vivo</i> quantification of contrast agent concentration using the induced magnetic field for timeâ€resolved arterial input function measurement with MRI. Medical Physics, 2008, 35, 5328-5339.	1.6	66
11	Unambiguous identification of superparamagnetic iron oxide particles through quantitative susceptibility mapping of the nonlinear response to magnetic fields. Magnetic Resonance Imaging, 2010, 28, 1383-1389.	1.0	57
12	Effective motionâ€sensitizing magnetization preparation for black blood magnetic resonance imaging of the heart. Journal of Magnetic Resonance Imaging, 2008, 28, 1092-1100.	1.9	51
13	Quantitative Susceptibility Mapping (QSM) Algorithms: Mathematical Rationale and Computational Implementations. IEEE Transactions on Biomedical Engineering, 2017, 64, 2531-2545.	2.5	49
14	Magnetic susceptibility matching at the air-tissue interface in rat lung by using a superparamagnetic intravascular contrast agent: Influence on transverse relaxation time of hyperpolarized helium-3. Magnetic Resonance in Medicine, 2005, 54, 28-33.	1.9	27
15	Phase-contrast velocimetry with hyperpolarized3He for in vitro and in vivo characterization of airflow. Magnetic Resonance in Medicine, 2006, 55, 1318-1325.	1.9	27
16	Velocity-selective RF pulses in MRI. Magnetic Resonance in Medicine, 2006, 55, 171-176.	1.9	26
17	Clinical Integration of Automated Processing for Brain Quantitative Susceptibility Mapping: Multiâ€Site Reproducibility and Singleâ€Site Robustness. Journal of Neuroimaging, 2019, 29, 689-698.	1.0	22
18	European Ultrahighâ€Field Imaging Network for Neurodegenerative Diseases (EUFIND). Alzheimer's and	1.2	17

¹⁸ Dementia: Diagnosis, Assessment and Disease Monitoring, 2019, 11, 538-549.

#	Article	IF	CITATIONS
19	2D harmonic filtering of MR phase images in multicenter clinical setting: Toward a magnetic signature of cerebral microbleeds. NeuroImage, 2015, 104, 287-300.	2.1	16
20	Aerosol deposition in the lungs of spontaneously breathing rats using Gdâ€DOTAâ€based contrast agents and ultraâ€short echo time MRI at 1.5 Tesla. Magnetic Resonance in Medicine, 2016, 75, 594-605.	1.9	16
21	A new paradigm for lung-conservative total liquid ventilation. EBioMedicine, 2020, 52, 102365.	2.7	16
22	Comparison of fast field-cycling magnetic resonance imaging methods and future perspectives. Molecular Physics, 2019, 117, 832-848.	0.8	15
23	Sources of systematic error in proton density fat fraction (PDFF) quantification in the liver evaluated from magnitude images with different numbers of echoes. NMR in Biomedicine, 2018, 31, e3843.	1.6	14
24	Simultaneous pressure–volume measurements using optical sensors and MRI for left ventricle function assessment during animal experiment. Medical Engineering and Physics, 2015, 37, 100-108.	0.8	13
25	Estimating absolute aortic pressure using MRI and a one-dimensional model. Journal of Biomechanics, 2014, 47, 3390-3399.	0.9	12
26	Improved cerebral microbleeds detection using their magnetic signature on T2*-phase-contrast: A comparison study in a clinical setting. NeuroImage: Clinical, 2017, 15, 274-283.	1.4	11
27	Clinical Integration of Quantitative Susceptibility Mapping Magnetic Resonance Imaging into Neurosurgical Practice. World Neurosurgery, 2019, 122, e10-e19.	0.7	10
28	Simultaneous proton density, T ₁ , T ₂ , and flipâ€angle mapping of the brain at 7 T using multiparametric 3D SSFP imaging and parallelâ€transmission universal pulses. Magnetic Resonance in Medicine, 2020, 84, 3286-3299.	1.9	8
29	Magnetic source MRI: A new quantitative imaging of magnetic biomarkers. , 2009, 2009, 53-6.		7
30	Evaluation of lung recovery after static administration of three different perfluorocarbons in pigs. BMC Pharmacology & Toxicology, 2014, 15, 53.	1.0	6
31	Simultaneous multi-parametric mapping of total sodium concentration, T1, T2 and ADC at 7â€ [−] T using a multi-contrast unbalanced SSFP. Magnetic Resonance Imaging, 2018, 53, 156-163.	1.0	5
32	Quantitative Gdâ€ĐOTAâ€based aerosol deposition mapping in the lungs of asthmatic rats using 3D UTEâ€MRI. NMR in Biomedicine, 2018, 31, e4013.	1.6	4
33	Design of a fast field-cycling magnetic resonance imaging system, characterization and methods for relaxation dispersion measurements around 1.5 T. Review of Scientific Instruments, 2020, 91, 024102.	0.6	3
34	Phase contrast MRI for discriminating brain microbleed in a multicentre clinical study. , 2014, , .		1
35	Molecular Imaging to Predict Response to Targeted Therapies in Renal Cell Carcinoma. Contrast Media and Molecular Imaging, 2017, 2017, 1-8.	0.4	1
36	Phase-contrast velocity mapping for highly diffusive fluids: Optimal bipolar gradient pulse parameters for hyperpolarized helium-3. Magnetic Resonance in Medicine, 2014, 72, 1072-1078.	1.9	0

#	Article	IF	CITATIONS
37	Molecular Magnetic Resonance and Ultra Sound Imaging of Tumor Angiogenesis. International Journal of Radiology and Imaging Technology, 2017, 3, .	0.1	0